ELSEVIER

Journal of Power Sources 93 (2001) 258–267

JOURNAL OF POWER SOURCES

www.elsevier.com/locate/jpowsour

Short communication

Effect of radiation shield on pressure losses and power output of AMTEC cell

M.A.K. Lodhi*, A. Daloglu

Department of Physics, Texas Tech University, Lubbock, TX 79409, USA

Received 22 June 2000; accepted 27 June 2000

Abstract

Pressure loss in a PX-3A alkali metal thermo-electric converter (AMTEC) cell was investigated by varying the heat radiation between the beta alumina solid electrolyte (BASE) and the condenser. Chevron radiation shields were used to change the heat radiation between the BASE and the condenser in different numbers and at different angles. Results show that the pressure losses and also the pressure on the cathode side increase using chevron shields. The cell electrical power output and the cell efficiency decrease as the pressure on the cathode side increases when chevron shields are placed. The power output and efficiency increase as the chevron angle increases up to a certain limit.

Keywords: AMTEC; Pressure losses; Power output; Efficiency; Chevron radiation shields

1. Introduction

The alkali metal thermo-electric converter (AMTEC) is receiving increasing attention as a direct energy conversion device for high efficiency and high power density [1–28]. It has high conversion efficiency compared to the other thermoelectric energy converters. It can provide efficiency close to the theoretical Carnot efficiency at relatively low temperatures. However, efficiencies for AMTEC currently achieved are limited to 15–20%. The high efficiency and high power density of AMTEC at relatively high heat-rejection temperatures, around 600 K, and low heat source temperatures, below 1200 K, make it an attractive option for space missions, air force applications and many terrestrial purposes. In the space exploration field, the planetary exploration missions have so far used thermoelectric energy conversion devices which have relatively low conversion efficiency (∼5–7%) compared to AMTEC. Accordingly, those missions required a larger and heavier general purpose heat source (GPHS). AMTEC being four to six times more efficient [5] would require less amount of plutonium for GPHS, thus reducing the power system's mass by about 60%. It is expected that the continued interest in AMTEC cells will improve their efficiency, power density and reduce their time-dependent degradation.

The Air Force Research Laboratory (AFRL) has been operating AMTEC as test cells in a vacuum environment since 1997. They are being manufactured by Advanced Modular Power Systems Inc. (AMPS) with design input from Orbital Sciences Corporation (OSC), Nichols Research Corporation (NRC) and AFRL. These tests are performed in a prototypical environment to evaluate design modifications, identify performance, and establish an endurance data-base.

Typical AMTEC cells operate in three sodium vapor flow regimes, continuum, slip, and free molecular. Dushman [29] categorized the flow of gases into three regions and showed that it depends on the dimensionless Knudsen number K_n, the ratio of the mean free path to characteristic length. The three aforementioned regimes are arbitrarily determined as follows:

1. Continuum (viscous): $K_n \leq 0.01$.
2. Slip (transition): $0.01 < K_n < 1$.
3. Free molecular (molecular): $K_n \geq 1$.

Because of the complexity of the cell geometry and of these flow regimes, there were only limited studies to calculate vapor pressure losses [30–34].

In the present study, the pressure losses on the cathode side of a multitube vapor-anode AMTEC cell are calculated using the model, in which the flow coefficients in the free-molecular regime were calculated using the Dushman [29] formulas.

* Corresponding author. Tel.: +1-806-742-3778; fax: +1-806-742-1182.
E-mail address: b5mak@ttacs.ttu.edu (M.A.K. Lodhi).

0378-7753/01/$ – see front matter
PII: S0378-7753(00)00543-7

Nomenclature

$\bar{A}_k$	effective annulus flow area (m^2)
D	flow diffusion coefficient (m^2/s)
D_e	equivalent hydraulic diameter (m)
L	effective flow path through chevrons (m)
M	molecular weight of sodium ($M = 23$ g/mol)
$\dot{m}_z$	sodium vapor mass flow rate (kg/s)
$\dot{m}''_z$	sodium vapor mass flux (kg/m^2 s)
P_{out}	electrical energy generated by the cell (W)
R_g	perfect gas constant (8.314 J/mol K)
T	temperature (K)
x	distance from condenser (m)
z	axial coordinate (m)

Greek letters

$\bar{\alpha}_2$	coefficient for advection of axial momentum
χ	flow conductance of chevron shield (m^2/s)
μ	absolute viscosity of sodium vapor (kg/m s)
θ	angle of conical chevrons
ρ	density of sodium vapor (kg/m^3)

Those in the continuum regime were determined using an exact analytical solution (when available) or the equivalent hydraulic diameter approximation. The dusty-gas-model (DGM) was used to calculate the flow diffusion coefficients for all vapor pressures and flow regimes (free-molecular, transition, and continuum). The present vapor pressure loss model was coupled to a one-dimensional AMTEC electrical model, which allows the current density to vary axially along the beta alumina solid electrolyte (BASE) tubes. The coupled cell model is used to calculate the pressure losses on the cathode side of the multitube AMTEC cell, and estimates the effect of conical chevrons shield on the vapor pressure losses. The purpose is to investigate the effect of the cathode pressure on the power output and the efficiency of the cell.

2. AMTEC PX-3A cell

A brief design description of the AMTEC cell and its working is given here. Fig. 1 shows a typical PX type AMTEC cell. Our investigations are directed to the PX-3A type cell which contains five BASE tubes in series and operates in a vapor–vapor mode, which means that sodium is in the vapor state on both the low and high pressure sides of the BASE. Liquid sodium is wicked from the condenser and evaporated to the vapor at the evaporator in the space also shared by the high pressure side (inside) of the BASE tubes. The BASE tubes have two thin, porous electrodes of TiN, anode and cathode, on the inner and outer surfaces, respectively. The inner and outer electrodes are each contacted by a current collector which collects electrons at the anode (high pressure side of the BASE), conducts them through an external load, and supplies them for recombination with the sodium ions at the cathode (low pressure side of the

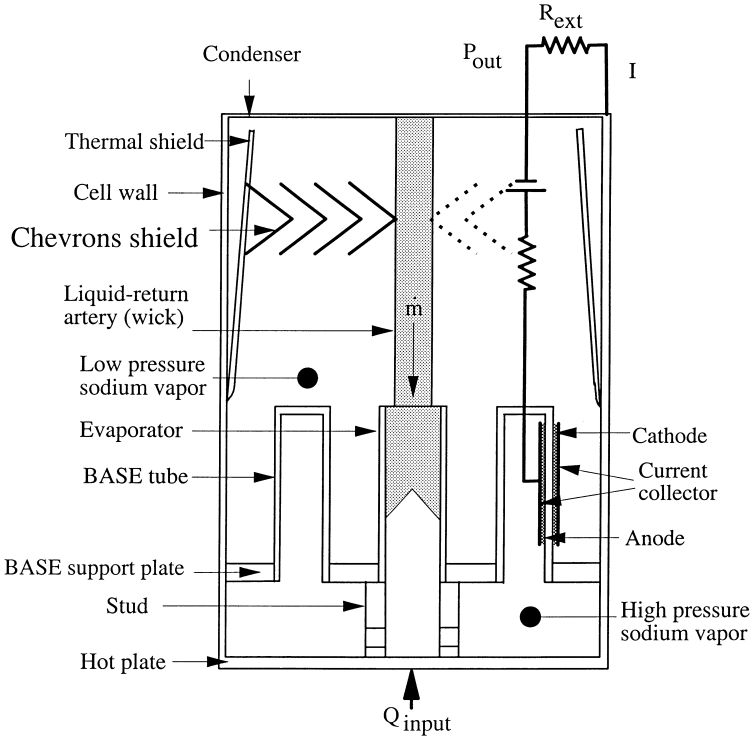

Fig. 1. A schematic diagram of vapor-anode AMTEC cell.

Table 1
Design parameters of the PX-3A cell

Cell diameter (mm)	31.75
Cell height (mm)	101.6
Evaporator type	Deep cone
Evaporator elevation (mm)	5.18
Evaporator standoff thickness (mm)	0.71
Evaporator standoff material	SS
Standoff rings (mm)	1.1
Ring material	Ni
Stud area (mm^2)	38
Stud material	SS
Number of BASE tubes	5
Tube length (mm)	32
Electrode/tube (mm^2)	600
Tube braze material	TiNi
Current collector	60-mesh Mo
Feedthrough braze	TiCuNi
Radiation shield type	Circular
Shield material	SS
Condenser type	Creare
Hot side	SS
Cell wall	SS
Initial test date	7/9/97
Operation (h)	18,000

BASE). The heat is supplied through the hot plate and the cell is operated in vacuum. The material and geometrical dimensions of this cell are given in Table 1.

3. Pressure losses on cathode side

In this study, the pressure drop along the BASE tubes, pressure loss due to sudden expansion at the top of the BASE tubes, pressure loss in annulus above the BASE tubes, and pressure loss due to vapor flow through chevrons shield are investigated. The sodium flow rate along the BASE tube is not constant. It increases because of continuous sodium addition at the BASE tubes outer surfaces. The sodium vapor pressure gradient along the BASE tubes, in the axial direction, is given by [34]

$$\frac{\mathrm{d}P}{\mathrm{d}z} = -\frac{1+\bar{\alpha}_2(\dot{m}_z''2/P)\{(1/T)(\mathrm{d}T/\mathrm{d}z)+(2/\dot{m}_z'')(\mathrm{d}\dot{m}_z''/\mathrm{d}z)\}}{1-\bar{\alpha}_2(R_\mathrm{g}T/M)(\dot{m}_z''/P)^2} \times \frac{R_\mathrm{g}T}{M}\frac{\dot{m}_z''}{D} \quad (1)$$

where D is the diffusion coefficient, R_g the perfect gas constant, M the molecular weight of sodium, T the temperature of sodium vapor, $\bar{\alpha}_2$ the coefficient for advection of axial momentum, and where $\dot{m}''$ is the sodium vapor axial mass flux. This equation is integrated numerically to obtain the sodium vapor pressure along the BASE tubes.

The pressure drop due to sudden expansion at the top of the BASE tubes is calculated from [35]

$$\Delta P = K\frac{1}{2}\left(\frac{\dot{m}_z''2}{\rho}\right) \quad (2)$$

where K is a dimensionless quantity calculated from the resistance coefficient, ξ, and Reynolds number given by

$$K = \xi\left(\frac{\mu}{D_\mathrm{e}\dot{m}_z''}\right) \quad (3)$$

$$K = \frac{\xi}{Re} \quad (4)$$

where the Reynolds number Re is given by

$$Re = \frac{\rho D_\mathrm{e} V}{\mu} \quad (5)$$

where D_e is the equivalent hydraulic diameter. The resistance coefficient ξ is given as a function of expansion area ratio [35], μ is the absolute viscosity and ρ is the density of sodium vapor.

The sodium vapor pressure gradient in the annulus above the BASE tubes is given similar to the sodium vapor pressure gradient along the BASE tubes. Because of constant sodium flow rate in this region, Eq. (1) becomes

$$\frac{\mathrm{d}P}{\mathrm{d}z} = \frac{1+\bar{\alpha}_2(\dot{m}_z''2/P)\{(1/T)(\mathrm{d}T/\mathrm{d}z)\}}{1-\bar{\alpha}_2(R_\mathrm{g}T/M)(\dot{m}_z''/P)^2}\frac{R_\mathrm{g}T}{M}\frac{\dot{m}_z''}{D} \quad (6)$$

This equation is integrated numerically to obtain the sodium vapor pressure in the annulus above the BASE tubes.

When N number of conical chevrons are used in the chevron shield, there are $N-1$ conical flow passages between the chevrons. The expression for pressure loss through the chevrons is given as [34]

$$\Delta P = \frac{1}{\chi}\left(\frac{R_\mathrm{g}T}{M}\right)\dot{m}_z, \quad \text{where } \chi = \sum_{k=1}^{N-1}\frac{\bar{A}_k\bar{D}_k}{L} \quad (7)$$

where $\dot{m}_z$ is the sodium vapor axial mass flow rate, L the effective flow path through the chevrons, $\bar{A}_k$ the effective annulus flow area, and where $\bar{D}_k$ is the flow coefficient for the flow in the annulus.

4. Results and discussion

The multitube, vapor-anode AMTEC cell analyzed here has a hot plate kept at a temperature of 1173 K, and a condenser at a temperature of 623 K. This cell contains a radiation shield, laid against the cell wall above the BASE tubes, to reduce parasitic heat losses through the cell wall. The temperature-independent exchange current and contact resistance between current collector and electrode were taken to be 120 A $K^{1/2}$/Pa m^2 and 0.08 Ω cm^2, respectively [36]. When the external load resistance, $R_\mathrm{load} = 1\,\Omega$, it almost gives the maximum electrical power output. Additional to radiation shield, a chevron radiation shield system consisting of different numbers of chevrons at different angles has been considered above the BASE tubes and analyzed for the sodium vapor pressure, and thus, the power output and efficiency.

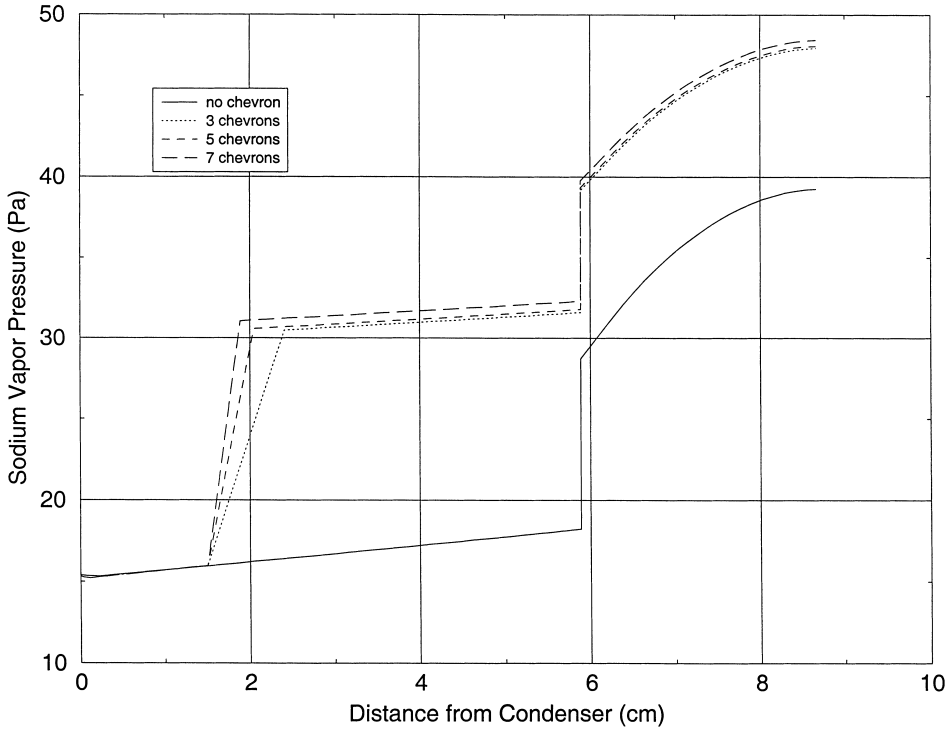

Fig. 2. Sodium vapor pressure on the cathode side of a multitube AMTEC cell ($\theta = 45°$, clearance = 15 mm).

Fig. 2 shows the calculated sodium vapor pressure on the cathode side of the AMTEC cell for different numbers of chevrons. When any number of chevrons are used, the cathode-side pressure of sodium vapor increases by almost 10 Pa compared to the situation with no chevron. This pressure increases with increasing chevron numbers. The sodium flow rate depends slightly on chevron numbers as seen in Fig. 3. The sodium flow rates for different numbers

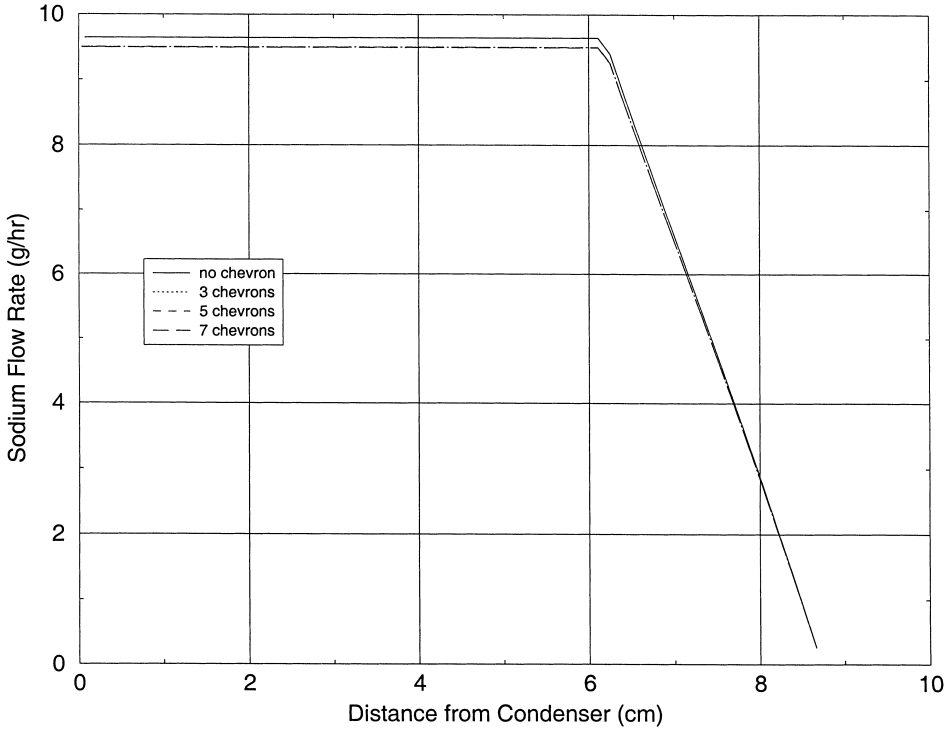

Fig. 3. Sodium flow rate ($\theta = 45°$, clearance = 15 mm).

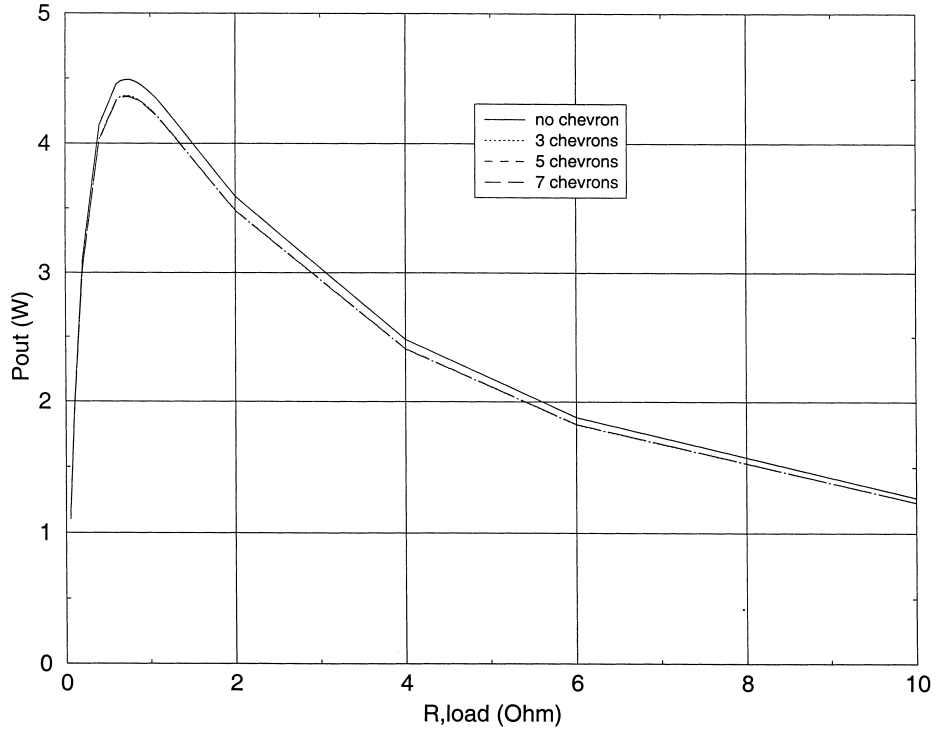

Fig. 4. Effects of chevron numbers on cell electrical power output ($\theta = 45°$, clearance = 15 mm).

of chevrons are almost the same, but are about 1.5% less than the situation of no chevron. The effects of the chevron numbers on the cell electrical power output and cell conversion efficiency are illustrated in Figs. 4 and 5, respectively. For cell efficiency, the effect of the chevrons on the heat radiation between BASE and condenser is neglected. Computer simulation of the AMTEC cell shows that the heat loss to the condenser due to the heat radiation from the

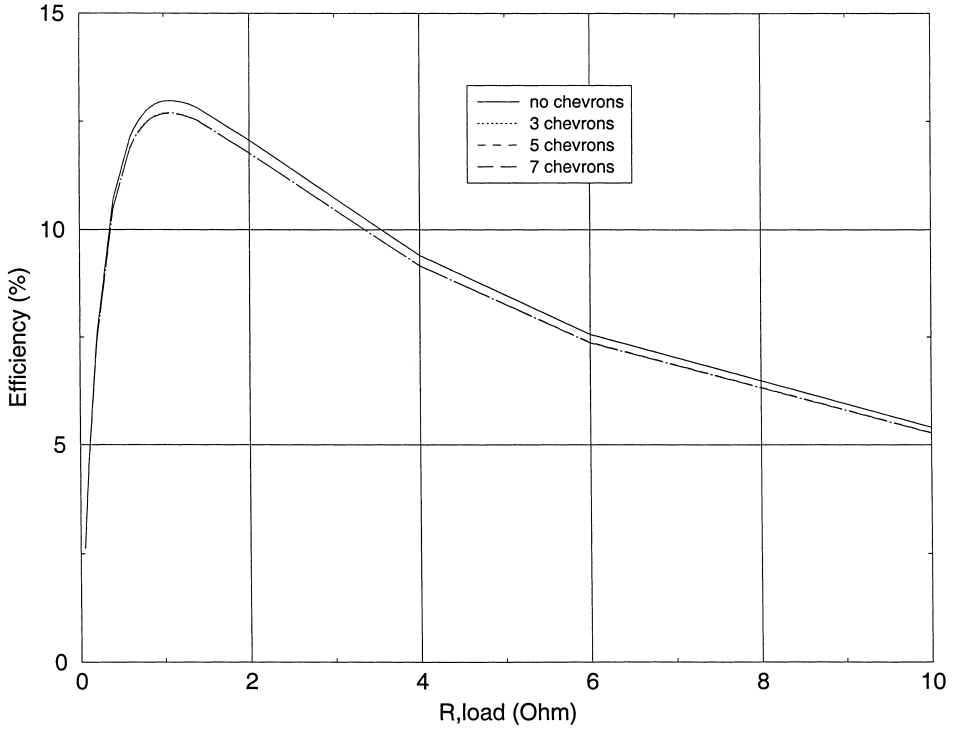

Fig. 5. Effects of chevron numbers on cell efficiency ($\theta = 45°$, clearance =15 mm).

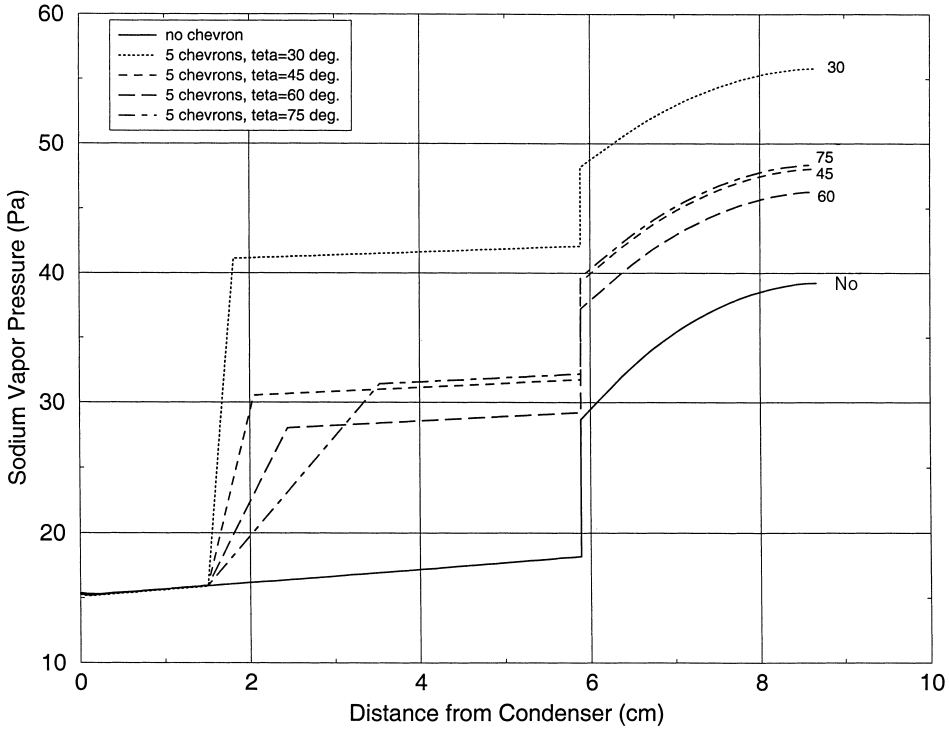

Fig. 6. Sodium vapor pressure on the cathode side of a multitube AMTEC cell (five chevrons, clearance = 15 mm).

BASE to the condenser is smaller than the other heat losses [37,38]. The cell gives smaller electrical power output and conversion efficiency when the chevron heat shield is placed.

The effects of the chevron angle on the sodium vapor pressure using five chevrons are given in Fig. 6. Small chevron angles give a larger pressure drop for the flow through chevrons. The pressure drop first decreases with

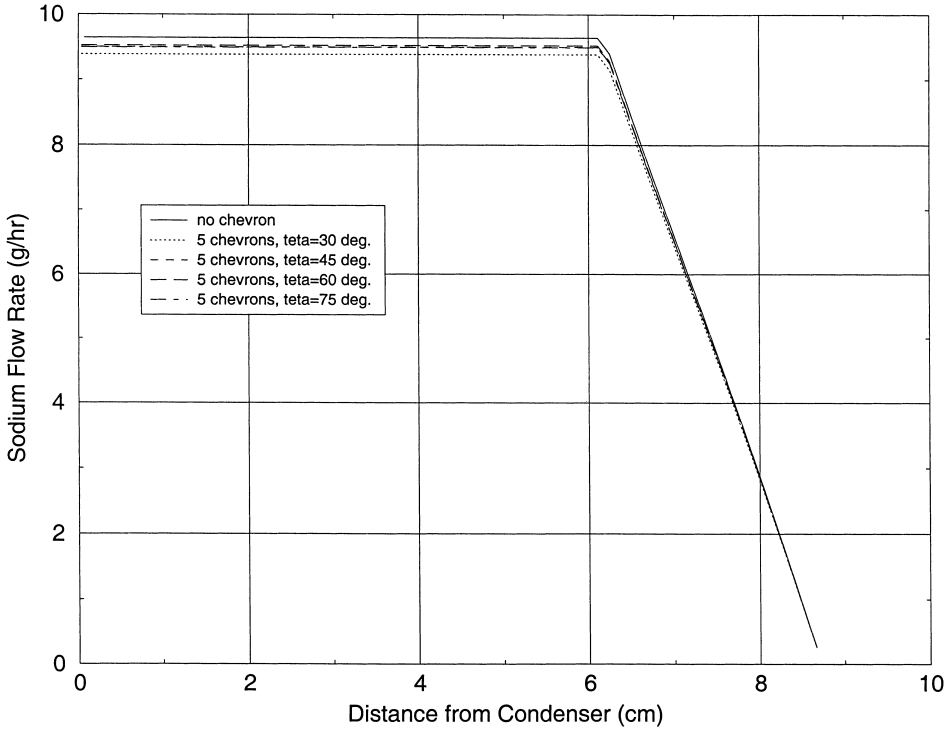

Fig. 7. Sodium flow rate (five chevrons, clearance = 15 mm).

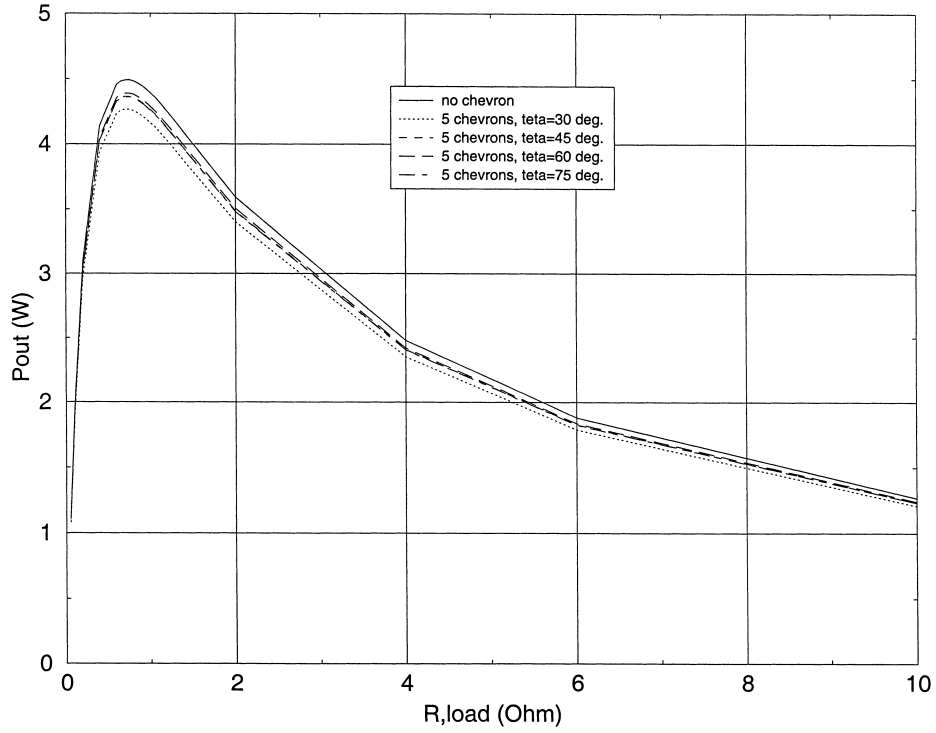

Fig. 8. Effects of chevron angles on cell electrical power output (five chevrons, clearance = 15 mm).

increasing chevron angle, but after 60°, it starts increasing. Sodium flow rate shows a trend similar to the one shown by the sodium vapor pressure (pressure drop through chevrons) with changing chevron angle (see Fig. 7). The cell electrical power output and cell conversion efficiency depend on chevron angle as shown in Figs. 8 and 9. In these cases also, the larger values are for no chevron. At smaller chevron angle, the cell electrical power output and cell conversion

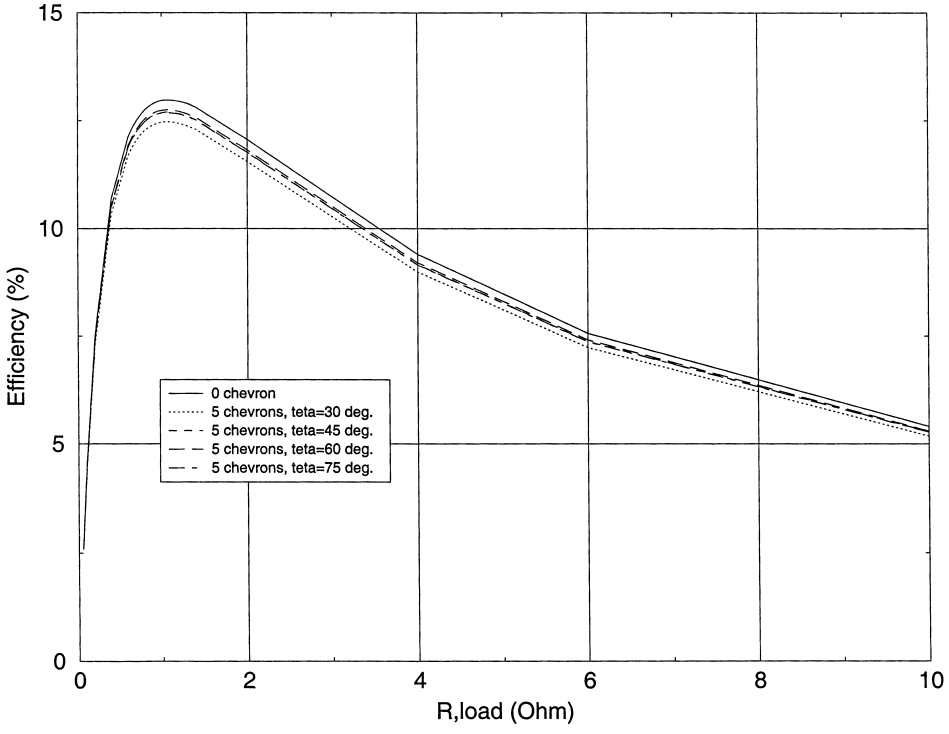

Fig. 9. Effects of chevron angles on cell efficiency (five chevrons, clearance = 15 mm).

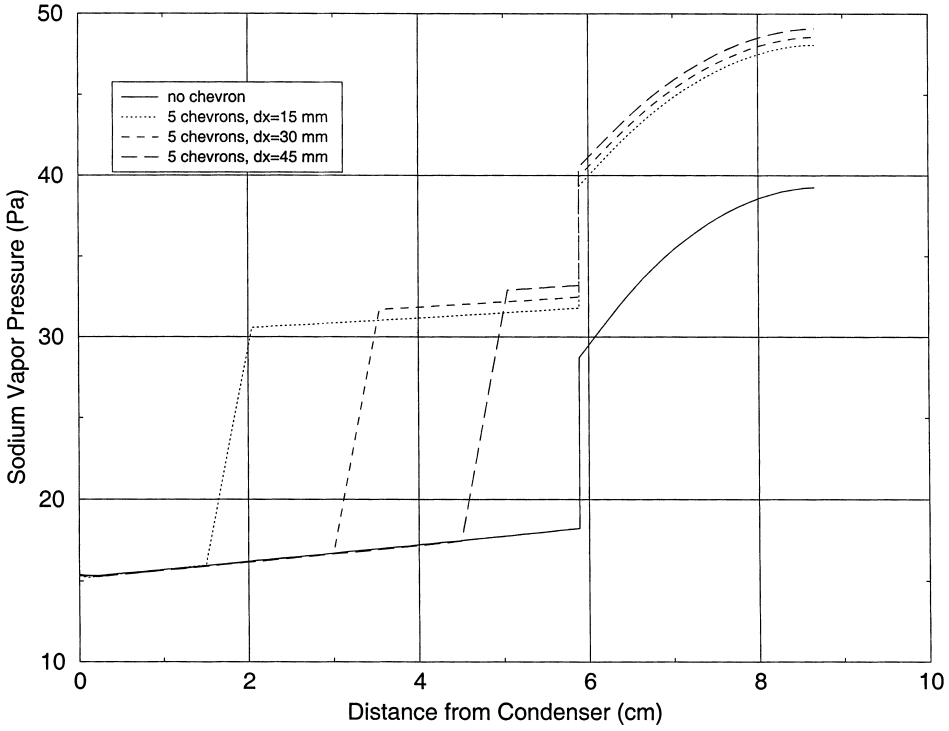

Fig. 10. Sodium vapor pressure on the cathode side of a multitube AMTEC cell (five chevrons, $\theta = 45^\circ$).

efficiency are smaller. The cell electrical power output and efficiency increase with increasing chevron angle, and start decreasing after 60° following the opposite trend of the pressure drop.

Fig. 10 shows the effects of the clearance between the top of the chevron shield and the condenser on sodium vapor pressure. Pressure losses through chevrons increase with increasing clearance, because the vapor temperature

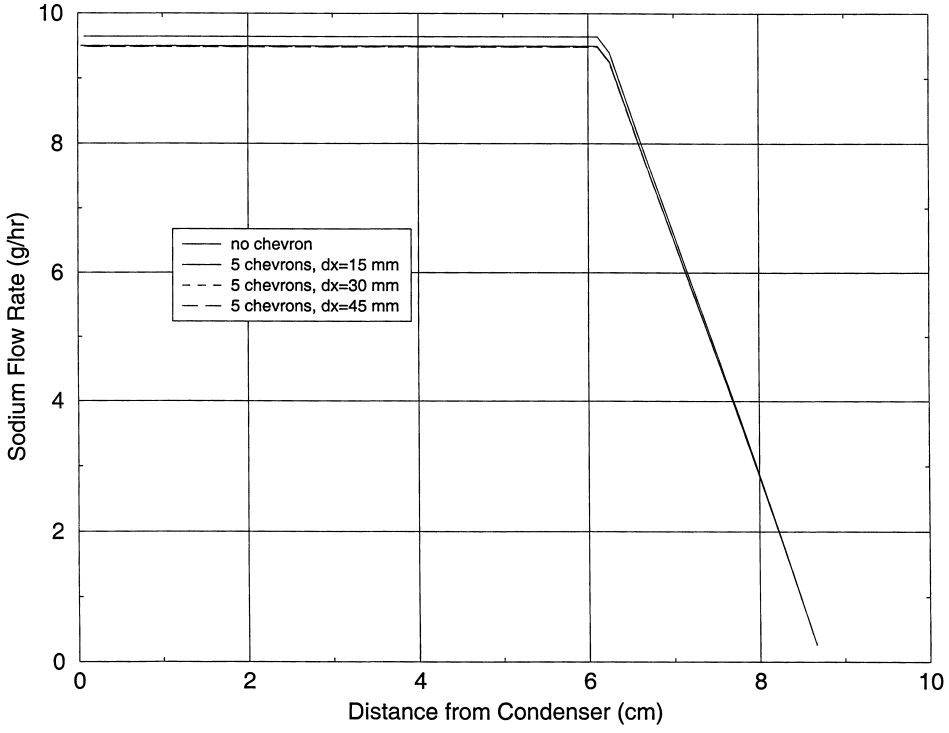

Fig. 11. Sodium flow rate (five chevrons, $\theta = 45^\circ$).

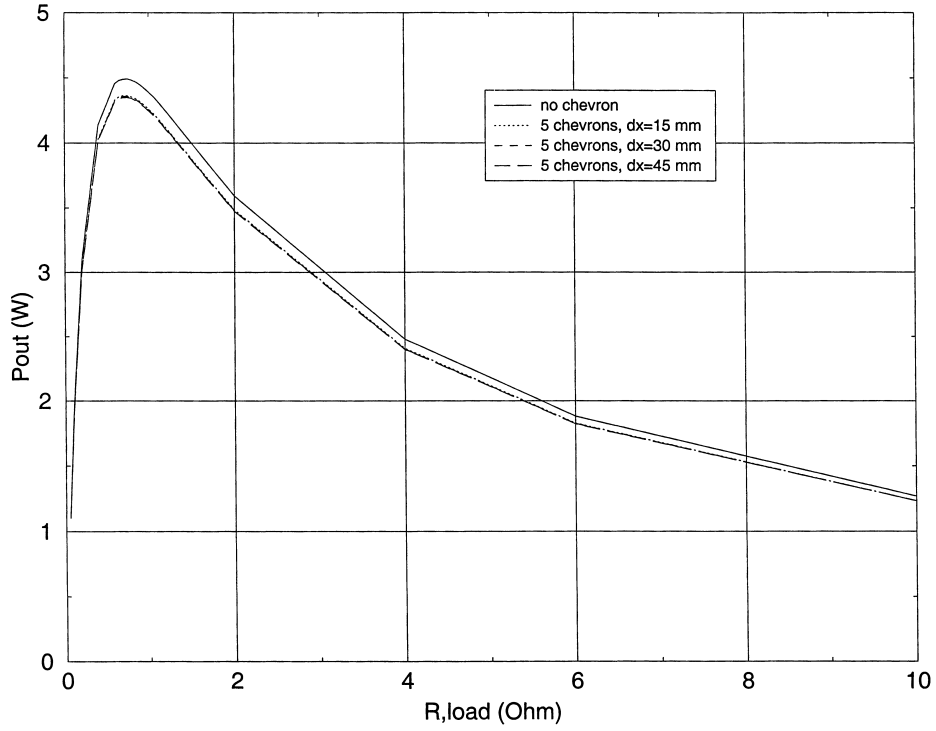

Fig. 12. Effects of clearance between condenser and chevrons shield on the cell electrical power output (five chevrons, $\theta = 45^{\circ}$).

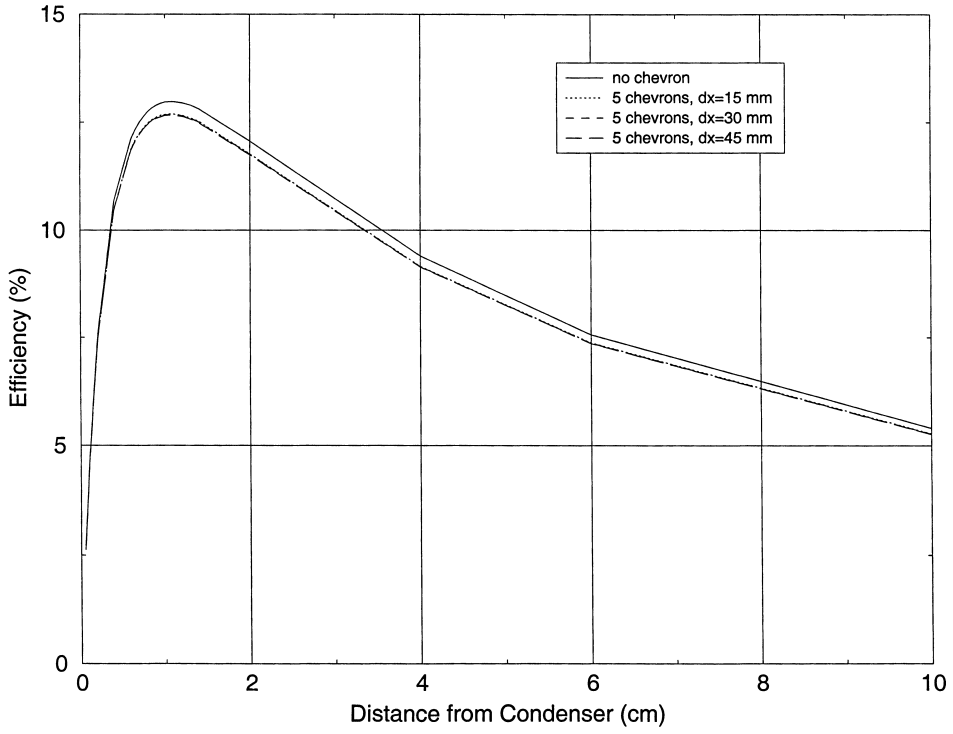

Fig. 13. Effects of clearance between condenser and chevrons shield on the cell efficiency (five chevrons, $\theta = 45^{\circ}$).

increases when the chevron shield gets closer to the BASE tubes. The effects of the clearance between the top of the chevron shield and the condenser on sodium flow rate, cell electrical power output, and cell efficiency are not noticeable (Figs. 11–13).

5. Conclusion

The results show that the sodium vapor pressure on the cathode side increases by almost 31% when a chevron shield system (five chevrons, a chevron angle of 45°, and a shield

clearance of 15 mm) is used. However, the changes in sodium flow rate, cell electrical power, and cell conversion efficiency are small. The cell electrical power output decreases only by about 3% as the cathode pressure increases to 31%. The motivation for placing some heat shield was to reduce the radiation losses which could allow better efficiency and power output. The introduction of heat shields caused the cathode pressure to increase which impeded the ion flow rate, thus affecting the power output somewhat adversely. It is therefore best not to introduce any chevron heat shield with the present design of AMTEC PX-3A version.

Acknowledgements

This work is supported in parts by the United States Air Force Office of Scientific Research via Sub-contract No. F99-0832 CFDA# 12800, Grant No. 98-0001 and the Texas Higher Education Coordinating Board Grant No. ATP 003644-091.

References

[1] J.T. Kummer, N. Weber, US Patent 3,458,356 (1968), assigned to Ford Motor Co.
[2] N. Weber, Energy Conversion 14 (1974) 1.
[3] T.K. Hunt, N. Weber, T. Cole, in: Proceedings of the 10th Intersociety Energy Conversion Engineering Conference, Part 2, 1975, p. 231.
[4] T.K. Hunt, N. Weber, T. Cole, in: Proceedings of the 13th Intersociety Energy Conversion Engineering Conference, SAE, Warrandale, PA, 1978, p. 2001.
[5] A. Schock, in: Proceedings of the 15th Intersociety Energy Conversion Engineering Conference, SAE, Seattle, WA, 1980, p. 1032.
[6] T.K. Hunt, N. Weber, T. Cole, in: J.B. Bates, G.C. Ferrington (Eds.), Solid State Ionics, North-Holland, Amsterdam, 1981, p. 263.
[7] G. Crosbie, G. Tennenhouse, J. Am. Ceram. Soc. 65 (1982) 187.
[8] T. Cole, Science 221 (1983) 915.
[9] C.P. Bankston, T. Cole, S.K. Khanna, A.P. Thakoor, in: M.S. El-Genk, M.D. Hoover (Eds.), Space Nuclear Power Systems 1984, Vol. II, Orbit Book Co., Malabar, FL, 1985, p. 393.
[10] R.M. Williams, S.K. Khanna, C.P. Bankston, A.P. Thakoor, T. Cole, J. Electrochem. Soc. 133 (1986) 1587.
[11] R.M. Williams, B.L. Wheeler, B. Jeffries-Nakamura, M.E. Loveland, C.P. Bankston, T. Cole, J. Electrochem. Soc. 135 (1988) 2736.
[12] R.K. Sievers, C.P. Bankston, in: Proceedings of the 23rd Intersociety Energy Conversion Conference, Vol. 3, 1988, p. 159.
[13] M.L. Underwood, D. O'Connor, R.M. Williams, B. Jeffries-Nakamura, C.P. Bankston, in: Proceedings of the 24th Intersociety Energy Conversion Engineering Conference, Washington, DC, Vol. 6, 1989, p. 2833.
[14] R.M. Williams, B. Jeffries-Nakamura, M.L. Underwood, B.L. Wheeler, M.E. Loveland, S.J. Kikkert, J.L. Lamb, J.T. Kummer, C.P. Bankstone, J. Electrochem. Soc. 136 (1989) 893.
[15] R.M. Williams, M.E. Loveland, B. Jeffries-Nakamura, M.L. Underwood, C.P. Bankston, H. Leduc, J.T. Kummer, J. Electrochem. Soc. 1709 (1990) 137.
[16] R.M. Williams, B. Jeffries-Nakamura, M.L. Underwood, C.P. Bankston, J.T. Kummer, J. Electrochem. Soc. 137 (1990) 1716.
[17] M.L. Underwood, D. O'Connor, R.M. Williams, B. Jeffries-Nakamura, M.A. Ryan, C.P. Bankston, J. Propulsion Power 84 (1992) 878–882.
[18] T.K. Hunt, R.K. Sievers, J.F. Ivaneok, J.E. Pantolin, D.A. Butkiewicz, in: Proceedings of the 28th Intersociety Energy Conversion Conference, Vol. 1, 1993, p. 849.
[19] C.P. Bankston, A Critical Review of Space Nuclear Power and Propulsion 1984–1993, AIP, New York, 1994, pp. 443–457.
[20] J.F. Ivanenok III, R.K. Sievers, C.J. Crowley, AIChE Symp. Ser. 91 (1995) 356.
[21] M.J. Schuller, R.A. LeMire, K. Horner-Richardson, in: Proceedings of the 30th Intersociety Energy Conversion Conference, Vol. 3, 1995, p. 159.
[22] T.K. Hunt, R.K. Sievers, J.F. Ivanenok, in: Proceedings of the 30th Intersociety Energy Conversion Conference, Vol. 3, 1995, p. 145.
[23] M.A.K. Lodhi, M. Schuller, P. Housgen, in: M.S. El-Genk (Ed.), Proceedings of the Space Technology and Applications International Forum, AIP, New York, 1996, p. 1285.
[24] Q. Ni, J. Tong, Y. Kan, J. Wang, Y. Cui, in: Proceedings of the 32nd Intersociety Energy Conversion Conference #97058, Vol. 2, 1997, p. 1180.
[25] A. Schock, H. Noravian, V. Kumar, C. Or, in: Proceedings of the 32nd Intersociety Energy Conversion Conference # 97529, Vol. 2, 1997, p. 1136.
[26] J.M. Merrill, M. Schuller, L. Huang, 15th STAIF, AIP, New York, 1998, p. 1613.
[27] J.M. Merrill, C. Mayberry, 16th STAIF, AIP, New York, 1999, p. 1369.
[28] A. Schock, H. Noravian, C. Or, V. Kumar, AIP Conference Proceedings, Vol. 158, 1999, p. 1534.
[29] S. Dushman, Scientific Foundations of Vacuum Technique, 2nd Edition, Wiley, New York, 1962.
[30] G.A. Johnson, in: M.S. El Genk (Ed.), Proceedings of the 11th Symposium on Space Nuclear Power and Propulsion, CONF-940101, Vol. 2, American Institute of Physics, New York, NY, AIP Conference Proceedings No. 301, 1994, pp. 581–585.
[31] J.F. Ivanenok III, R.K. Sievers, W.W. Schultz, in: M.S. El Genk (Ed.), 11th Symposium on Space Nuclear Power and Propulsion, CONF-940101, Vol. 3, American Institute of Physics, New York, NY, AIP Conference Proceedings No. 301, 1994, pp. 1501–1506.
[32] A. Schock, C. Or, in: M.S. El-Genk (Ed.), Proceedings of the Space Technology and Applications International Forum (STIF-97), CONF-97115, Vol. 3, American Institute of Physics, New York, NY, AIP Conference Proceedings No. 387, 1997, pp. 1381–1394.
[33] A. Schock, C. Or, in: M.S. El-Genk (Ed.), Proceedings of the Space Technology and Applications International Forum (STIF-97), CONF-97115, Vol. 3, American Institute of Physics, New York, NY, AIP Conference Proceedings No. 387, 1997, pp. 1395–1404.
[34] J.M. Tournier, M.S. El-Genk, in: Proceedings of the 15th Symposium on Space and Nuclear Power and Propulsion, 3rd Space Technology and Applications International Forum (STAIF-98), Albuquerque, NM, Vol. III, American Institute of Physics, New York, NY, AIP Conference Proceedings No. 420, 1998, pp. 1595–1606.
[35] I.E. Idelchik, Handbook of Hydraulic Resistance, 3rd Edition, CRC Press, Boca Raton, FL, 1994.
[36] J.M. Tournier, M.S. El-Genk, M. Schuller, P. Hausgen, in: M.S. El-Genk (Ed.), Proceedings of the Space Technology and Applications International Forum (STAIF-97), CONF-970115, Vol. 3, American Institute of Physics, New York, NY, AIP Conference Proceedings No. 387, 1997, pp. 1543–1552.
[37] M.A.K. Lodhi, A. Daloglu, J. Power Sources 85 (2000) 203.
[38] M.A.K. Lodhi, A. Daloglu, J. Power Sources, in press.